Biosensors and Bioelectronics 124–125 (2019) 191–198

Contents lists available at ScienceDirect

Biosensors and Bioelectronics

journal homepage: www.elsevier.com/locate/bios

Hierarchical bi-continuous Pt decorated nanoporous Au-Sn alloy on carbon fiber paper for ascorbic acid, dopamine and uric acid simultaneous sensing

Han Yang[a,b,1], Jie Zhao[c,1], Meijia Qiu[d], Peng Sun[a,b,*], Dongxue Han[e,f,**], Li Niu[e,f], Guofeng Cui[a,b,*]

[a] Key Laboratory for Polymeric Composite & Functional Materials of Ministry of Education, School of Chemistry, Sun Yat-sen University, Guangzhou 510275, PR China
[b] Key Laboratory of Low-carbon Chemistry & Energy Conservation of Guangdong Province, Sun Yat-sen University, Guangzhou 510275, PR China
[c] School of Mechanical and Automotive Engineering, South China University of Technology, Guangzhou 510640, PR China
[d] MOE Laboratory of Bioinorganic and Synthetic Chemistry, The Key Lab of Low-Carbon Chemistry and Energy Conservation of Guangdong Province, School of Chemistry, Sun Yat-sen University, 135, Xingang West Road, Guangzhou 510275, PR China
[e] Center for Advanced Analytical Science, c/o School of Chemistry and Chemical Engineering, Guangzhou University, Guangzhou 510006, PR China
[f] State Key Laboratory of Electroanalytical Chemistry, c/o Engineering Laboratory for Modern Analytical Techniques, Changchun Institute of Applied Chemistry, Chinese Academy of Science, Changchun, 130022, Jilin, PR China

ARTICLE INFO

Keywords:
Nanoporous Au-Sn Alloy
Pt decoration
Ascorbic acid
Dopamine
Uric acid
Bio-Electrochemical sensor

ABSTRACT

In this work, Pt nanoparticles modified nanoporous AuSn(Pt@NP-AuSn) alloy on Ni buffered flexible carbon fiber paper (CFP) is fabricated by a simple replacement reaction in which NP-AuSn is fabricated by controllable dealloy of electrodeposited Au-Sn alloy films. The as prepared Pt@NP-AuSn/Ni/CFP possesses hierarchical pore structure, high specific surface area and excellent catalytic activity. Due to the bi-functions of both the large surface area of nanoporous metal and macroporous of carbon fiber paper facilitating mass transfer, the Pt@NP-AuSn/Ni/CFP shows high sensitivity of detecting ascorbic acid (AA), dopamine (DA) and uric acid (UA), with sensitivities of 0.14 μA μM^{-1} cm^{-2}, 15.23 μA μM^{-1} cm^{-2}, 0.28 μA μM^{-1} cm^{-2} under the concentration ranging from 200 to 2000 μM, 1–10 μM, and 25–800 μM for AA, DA and UA, respectively. Further, the Pt@NP-AuSn/Ni/CFP possesses long-term stability of sensing AA, DA and UA and presents great anti-interference towards a variety of common compounds in body fluid. All of these results manifest the Pt@NP-AuSn/Ni/CFP can be a promising candidate for the application of the electrochemical sensor for simultaneous detection of AA, DA and UA.

1. Introduction

Nanoporous metal is a sponge like structure with nano-holes and ligaments that offers hundreds or even thousands times of effective surface area compared to bulk metal, which can provide much more possible active sites. Due to the abundant active sites, excellent electronic conductivity and quantities of nanochannels, nanoporous metal has been considered as an ideal material for the application of supercapacitors (Lang et al., 2011; Zhang et al., 2016a), fuel cells (Liu et al., 2016; Xiao et al., 2017) and especially for electrochemical sensors (Feng et al., 2011; Wang et al., 2016; Xia et al., 2011; Zhang et al., 2016b).

It is well known that to some extent most of diseases demonstrate signals by expression of three important substances concentrations: ascorbic acid (AA), dopamine (DA) and uric acid (UA), of which the content variation can be in situ monitored and used to diagnose the disease like mental illness, AIDS and Parkinsonism (Jindal et al., 2014; Kim et al., 2016; Levine et al., 1991; Li et al., 2016; Sun et al., 2011a). AA, also called vitamin C, is an indispensable nutrient, commonly involves in the repair of tissue and the synthesis of certain neurotransmitters (Levine et al., 1991). DA is a vital neurotransmitter and chemical messenger in organism to maintain the normal functions of the nervous system (Li et al., 2016). UA is the final metabolite of purine, usually existing in serum and urine. In healthy human body fluid, UA kept constant at a certain value (Huang et al., 2002). Deviation from this value could result in illnesses like gout, hypertension and

* Corresponding authors at: Key Laboratory for Polymeric Composite & Functional Materials of Ministry of Education, School of Chemistry, Sun Yat-sen University, Guangzhou 510275, PR China.
** Corresponding author at: Center for Advanced Analytical Science, c/o School of Chemistry and Chemical Engineering, Guangzhou University, Guangzhou 510006, PR China.
E-mail addresses: sunp25@mail2.sysu.edu.cn (P. Sun), dxhan@gzhu.edu.cn (D. Han), cuigf@mail.sysu.edu.cn (G. Cui).
[1] These two authors contribute equally to this work.

https://doi.org/10.1016/j.bios.2018.10.012
Received 3 June 2018; Received in revised form 7 October 2018; Accepted 8 October 2018
Available online 13 October 2018
0956-5663/

hyperuricemia (Abellán-Llobregat et al., 2017a; Jindal et al., 2014). These three small organic molecules coexist in the body fluid and play basic roles in the course of biological metabolism. Therefore, simultaneously detecting UA, DA and AA in body fluid is of great importance for disease prevention, clinical diagnosis and scientific research. However, during the electrochemical testing, the oxidation potentials for UA, DA and AA are easily overlapped on ordinary solid electrode due to their adjacent oxidation potentials (Yue et al., 2014). Nanomaterials modification including noble metals (Abellán-Llobregat et al., 2017a, 2017b; Huang et al., 2014; Sun et al., 2011a, 2011b), metal oxides (Teymourian et al., 2013; Yue et al., n.d.), polymers (Kalimuthu and John, 2010; Lin et al., 2010) and carbon based nanomaterials (Cai et al., 2016; Deng et al., 2016; Jiang and Du, 2014; Yang and Li, 2014) have been employed to improve the selectivity and sensitivity of the AA, DA and UA. Three-dimensional nanoporous metal on porous substrate is expected to show high performance for the electrochemical detection of small biomolecules, due to the improved surface area and macroporous for mass transport. Through decorating nanoporous metal with some high performance metal particles or thin film such as Pt, the catalytic performance and selectivity towards UA, DA and AA were expect to obtain further elevation (Gao et al., 2017; Zhao et al., 2016).

In our previous work, strategy for fabricating the nanoporous gold (NPG) film on conductive substrate by chemically corroding the electrodeposited AuSn film was successfully proposed (Xu et al., 2014). It is an ideal method to prepare nanoporous gold films on a series of substrates under mild alkaline conditions. Up to now, we have successfully applied the NPG film on three dimensional nickel foam with hierarchical geometries in some electrochemical sensors and it demonstrated perfect catalytic performance (Ke et al., 2014b). Herein, we further modulated this method to synthesize nanoporous Au-Sn alloy with a little contents of Sn on a carbon fiber paper (CFP) by controlling the dealloying time. This hierarchical three-dimensional framework was further coated with a thin layer of Pt particles by replacing some redundant Sn in the nanoporous structure to fabricate the final electrode (Pt@NP-AuSn/Ni/CFP). The self-supported electrode shows excellent selectivity, sensitivity and detection limit for the simultaneously quantitative detection of UA, AA and DA.

2. Experimental

2.1. Reagent and chemical

Carbon fiber paper (CFP) was purchased from Toray Corp (TGP-H-090). Au–Sn alloy plating solution was obtained from Huizhou Leadao Electronic Material Co., Ltd (Huizhou, China, website: www.leadao.cn). Uric Acid (> 99%), dopamine (> 98%) and ascorbic acid (> 99%) were received from Aladdin Company. All other chemicals used in this investigation were of analytical grade without further purification.

2.2. Preparation of Ni/CFP

Ni film was coated on carbon fiber paper by an electrodeposition method. Details have been discussed in previous literature (Hua et al., 2012). Briefly, before the electrodeposition, carbon fiber paper (CFP) was treated in concentrated nitric acid at 115 °C for 80 min and immersed in 1 M NaOH to improve hydrophilic and remove organic binder on surface. Then the Ni layer was electrodeposited on activated CFP (10 mm × 10 mm) by constant current mode in a two-electrode electroplating configuration applying a cathodic current density of 3.8 mA cm^{-2} at 50 °C for 16 min.

2.3. Preparation of Pt@NP-AuSn/Ni/CFP electrode

The Pt@NP-AuSn/Ni/CFP was prepared by three steps. Firstly, The AuSn alloy (precursor of NP-AuSn) was electrodeposited on Ni coated CFP in AuSn alloy plating solution by constant current mode in a two-electrode electroplating configuration applying a current density of 5 mA cm^{-2} for 14 min at 45 °C. Secondly, the AuSn/Ni/CFP was immersed in etching solution (5 M NaOH and 0.1 M H_2O_2) for 20 h (leaving some Sn, this sample was named NP-AuSn/Ni/CFP). Thirdly, the NP-AuSn/Ni/CFP was washed with deionized water and immersed in 0.2 mM L^{-1} H_2PtCl_6 and 0.1 M $HClO_4$ solution for 1 h. After the replacement reaction, it was washed with abundant deionized water and dried in oven at 60 °C. Finally, the Pt@NP-AuSn/Ni/CFP can be synthesized.

2.4. Characterizations and electrochemical measurement

The surface morphologies of the samples were examined by field-emission scanning electron microscopy (SEM, Hitachi, SU8010, 10 keV) equipped with an energy dispersive spectrometer (EDS, IXRF). The composition of the samples was conducted on X-ray diffraction (XRD) (Rigaku D/max-2200/PC diffractometer) using Cu Ka radiation at a step rate of 8°/min. X-ray photoelectron spectroscopy (XPS) analysis was performed on a VG ESCALAB MK II with an Mg-Kα (1253.6 eV) achromatic X-ray source. Cyclic voltammetry (CV) and linear sweep voltammetry (LSV) were performed on Gamry Reference 600 electrochemical workstation and differential pulse voltammetry (DPV) was conducted on CHI-1230A electrochemical workstation. Both electrochemical measurements were carried out in a three-electrode setup with 0.1 M phosphate buffered saline (PBS) (pH = 7.0) as the electrolyte, Pt mesh electrode as the counter electrode and Ag-AgCl electrode as the reference electrode.

3. Results and discussion

3.1. Characterizations of the Pt@NP-AuSn/Ni/CFP

The initial attempts were conducted by directly electroplating AuSn alloy on carbon fiber paper. However, the binding force between these two materials seems rather weak and the AuSn layer was prone to be peeled off from the CFP. Fig. S1a shows the SEM image of the AuSn/CFP, which demonstrates that the fabricated AuSn alloy on CFP was rather rough and composed of large and coarse grains. To solve this problem and inspired by previous researchers (Ke et al., 2014b; Hua et al., 2012), a Ni layer was firstly pre-deposited on CFP as a buffer layer before the synthesis of AuSn alloy to enhance the weak adhesion force between AuSn alloy and CFP. After that, AuSn alloy with small grains and smoother surface could be uniformly electrodeposited on a nickel coated CFP substrate, as presented in Fig. S1b. Dealloying operation under adequate extent was then performed to obtain the nanoporous AuSn film with small amount of Sn content (named NP-AuSn/Ni/CFP). Finally, the redundant Sn contained in the nanoporous framework was replaced by a thin layer of Pt nanoparticles by simply soaking the NP-AuSn/Ni/CFP into H_2PtCl_6 based solution, finally acquiring the Pt@NP-AuSn/Ni/CFP electrode. The complete synthesized process is illustrated in the scheme of Fig. 1.

In our previous works, selectively etching Sn from AuSn alloy in alkaline conditions on Ni foam to form a three-dimensional nanoporous structure was successfully achieved (Ke et al., 2014a). With a little difference in this work, for the purpose of a Pt decoration, the Sn element in NP-AuSn/Ni/CFP wasn't completely removed by modulating the etching time to control the dealloying extent (Fig. S7d). Fig. 2a displays the SEM image of AuSn alloy film electrodeposited on the Ni buffered CFP. It can be seen that AuSn was fully distributed on the substrate with a compact structure. Subsequently, the typical SEM images of the AuSn alloy under an etching solution of 5 M NaOH and 0.1 M H_2O_2 for 20 h was shown in Fig. 2b, d. It can be clearly observed that the nanoporous AuSn alloy with a sponge-like structure is uniformly distributed on nickel-coated carbon fibers (Fig. 2d). The high-magnification SEM image (inset of Fig. 2d) reveals that the NP-AuSn film consists of bi-continuous nanostructures with interconnected

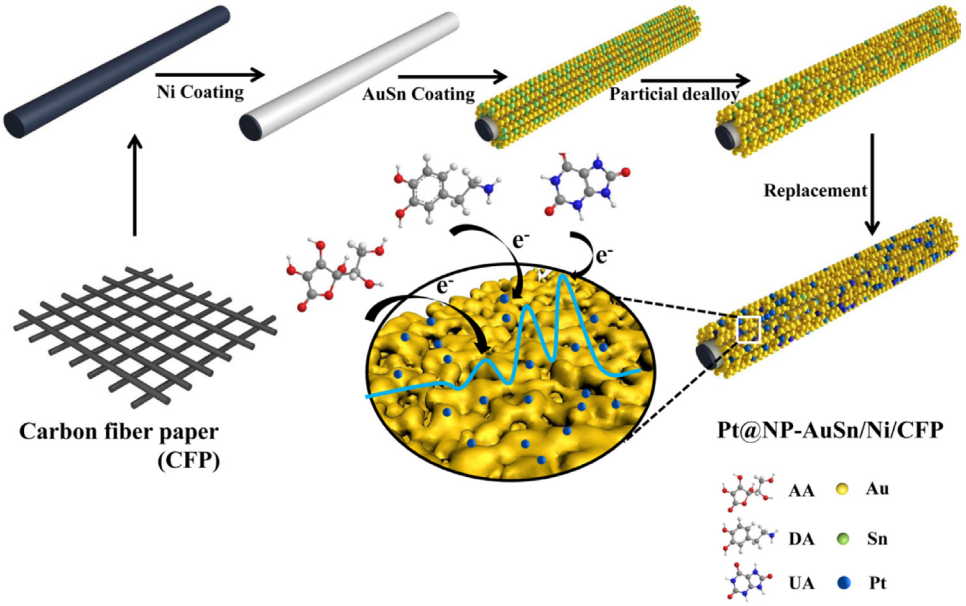

Fig. 1. Schematic illustration of the fabrication process for the Pt@NP-AuSn/Ni/CFP electrode and the corresponding detection mechanism.

ligaments and nanopores. The ligament size is about 50–10050–100 nm and the pore size is about 30–50 nm. With the process of dealloying reaction, the sample changes from silvery white to red brown (Fig. S6a-b), which is an indirect evidence of the dealloying process. Fig. 2c displays the SEM image of NP-AuSn/Ni/CFP soak in 0.2 mM H_2PtCl_6 and 0.1 M $HClO_4$ for 1 h, which indicate the three-dimensional structure still exists after the replacement reaction. The high-magnification SEM image shows the Pt particles are distributed on the ligaments of

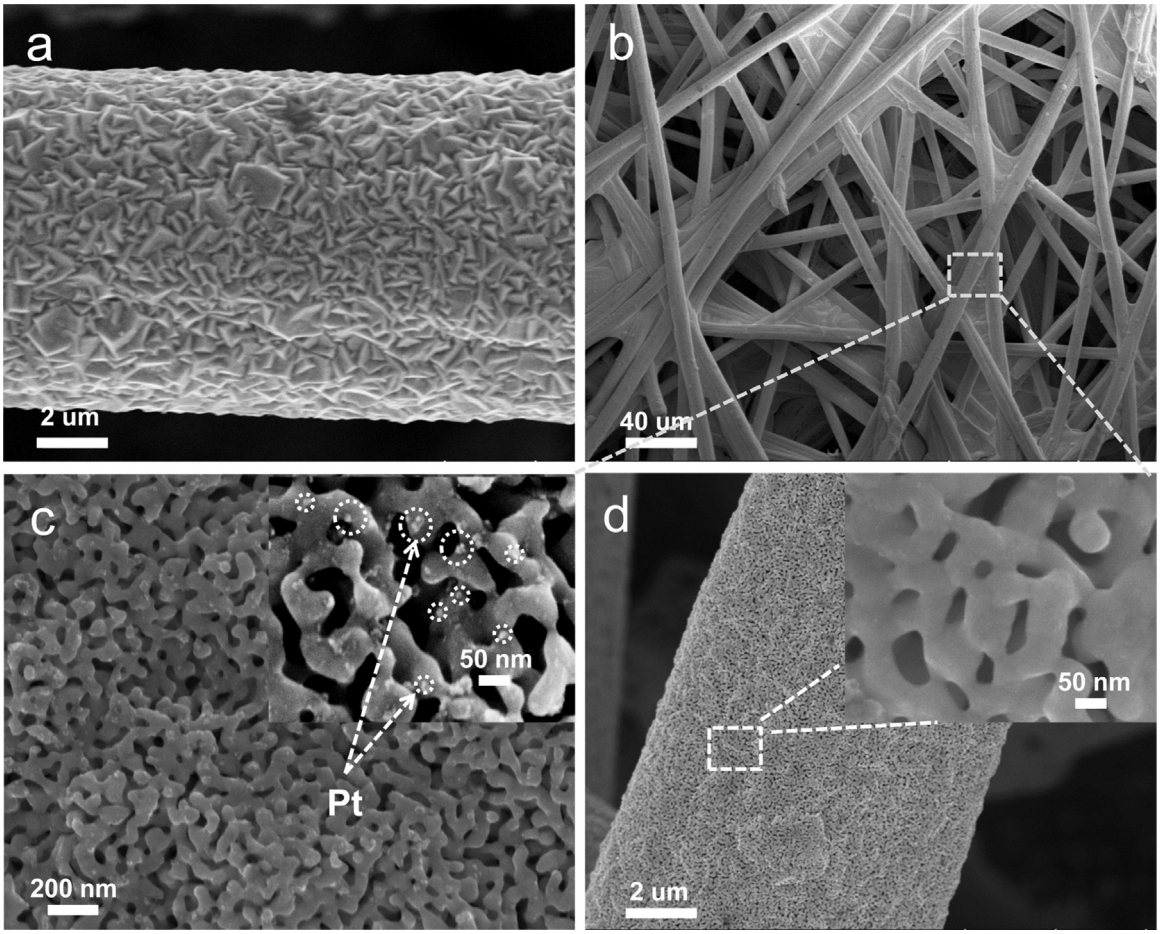

Fig. 2. SEM images of (a) AuSn alloy deposited on Ni buffered carbon fiber (b), (d) bi-continuous nanoporous AuSn film on Ni buffered carbon fiber and (c) Pt decorating nanoporous AuSn film on Ni buffered carbon fiber.

NP-AuSn with a size of 5–20 nm (inset of Fig. 2c). This obviously confirms the success of Pt decoration. The final sample of Pt@NP-AuSn/Ni/CFP is shown in the Supporting information which is red brown (Fig. S6c).

To further ascertain the detailed composition of the synthesized materials, EDS, XRD and XPS measurements were performed. Fig. S2a shows a typical EDS spectrum of AuSn/Ni/CFP, with the determined composition shown inset. It is clear that Au and Sn are the main components of AuSn/Ni/CFP (the C and Ni signal come from the carbon fiber substrate and Ni film on it), and Sn content occupies about 39.18% in atom ratio. Fig. S2b shows the EDS spectrum of NP-AuSn/Ni/CFP. It is shown that Sn content in NP-AuSn/Ni/CFP is reduced to a small amount of 4.28% in atom ratio (inset of Fig. S2a) as a result of the dealloying process. Fig. S3 shows the XRD patterns of the as-prepared Ni/CFP, AuSn/Ni/CFP and NP-AuSn/Ni/CFP. The results demonstrate that the as-prepared AuSn alloy film of AuSn/Ni/CFP and NP-AuSn/Ni/CFP is composed of two phases: Au_5Sn (JCPDS# 31-0568) and AuSn (JCPDS# 08-0463) which is in agreement with our previous work (Xu et al., 2014). However, Pt shows no distinct diffractions in Pt@NP-AuSn/Ni/CFP for its amorphous structure. In order to confirm that Pt was successfully decorated on NP-AuSn substrate, the XPS analysis was conducted. From the full spectrum survey in Fig. S4a, it can be clearly found that Sn, Au, Pt, Ni and C elements exist in this sample. Also the Au 4f, Pt 4f and Sn 3d spectra are presented in Fig. S4b and S4c, where the peak of Pt is rather low due to its small content.

For further ascertaining the successful coating of Pt on the NP-AuSn/Ni/CFP, electrochemical measurements were performed. Fig. S5 show the cyclic voltammetry curves of Pt@NP-AuSn/Ni/CFP and NP-AuSn/Ni/CFP in 0.5 M H_2SO_4. The NP-AuSn/Ni/CFP and Pt@NP-AuSn/Ni/CFP both show an obvious anodic current rising at approximately 1.2 V and a sharp cathodic peak at approximately 0.9 V, which ascribes to oxides formation and reduction on the surface of Au, respectively. Furthermore, a weak oxidation peak of 0.9 V and a reduction peak of 0.3 V only appear on the Pt@NP-AuSn/Ni/CFP electrode, which corresponding to the oxidation of the surface of Pt and the reduction of oxides respectively. The location of oxidation and reduction peaks for Au and Pt in Pt@NP-AuSn/Ni/CFP electrode are in good alignment with previous work (Cherevko et al., 2012). Thus, it is clear that NP-AuSn/Ni/CFP electrode was modified with a layer of Pt successfully.

3.2. Electrochemical behaviors of Pt@NP-AuSn/Ni/CFP

Fig. 3a-b shows the cyclic voltammetric response of CFP electrode and Pt@NP-AuSn/Ni/CFP electrode in PBS. For CFP electrode, broad and close oxidation peaks for signals of AA, DA and UA are presented, indicating that CFP lacks the ability to specifically recognize these three substances. However, for the Pt@NP-AuSn/Ni/CFP electrode, these three oxidation peaks were well separated. The oxidation peak of AA is located at 266 mV, which corresponds to the oxidation of hydroxyl groups to carbonyl groups in furan ring of AA on the surface of Pt@NP-AuSn/Ni/CFP (Khan et al., 2013; Yue et al., 2014). For DA, the appearance of a pair of redox peaks are located at 318 mV and 135 mV, corresponding to the two-electron oxidation of DA to dopaminoquinone and the reversible reduction from dopaminoquinone back to DA (Kim et al., 2014; Yue et al., 2014). The oxidation peak of UA is located at 446 mV, and no significant reduction peak appears, indicating that UA was oxidized to quinoxaline and underwent a rapid chemical reaction, which was considered to be an electrochemical reaction (EC) mechanism (Mirčeski and Lovrić, 2004; Yue et al., 2014; Zhao et al., 2015). AA, DA and UA molecules with different structures possess different absorption and oxidation behaviors on the electrode, and thus can be separated under different potential. In addition, the oxidation current density of the Pt@NP-AuSn/Ni/CFP electrode was enhances by a factor of 2–5 compared to that of the CFP electrode. The result could arise from following reasons: (i) The modification of the NP-AuSn improves the hydrophobic properties of carbon paper and enhances its reactivity in water environment. (ii) The macroporous structure of carbon paper facilitates mass transfer, thus enhancing the oxidation current. (iii) The NP-AuSn on surface offers numerous active sites and then increases catalytic area, thus enhancing the responsive signals. (iv) The higher catalytic activity of Pt compared with Au. The respond of CFP, Ni/CFP, NP-AuSn/Ni/CFP and Pt@NP-AuSn/Ni/CFP in PBS

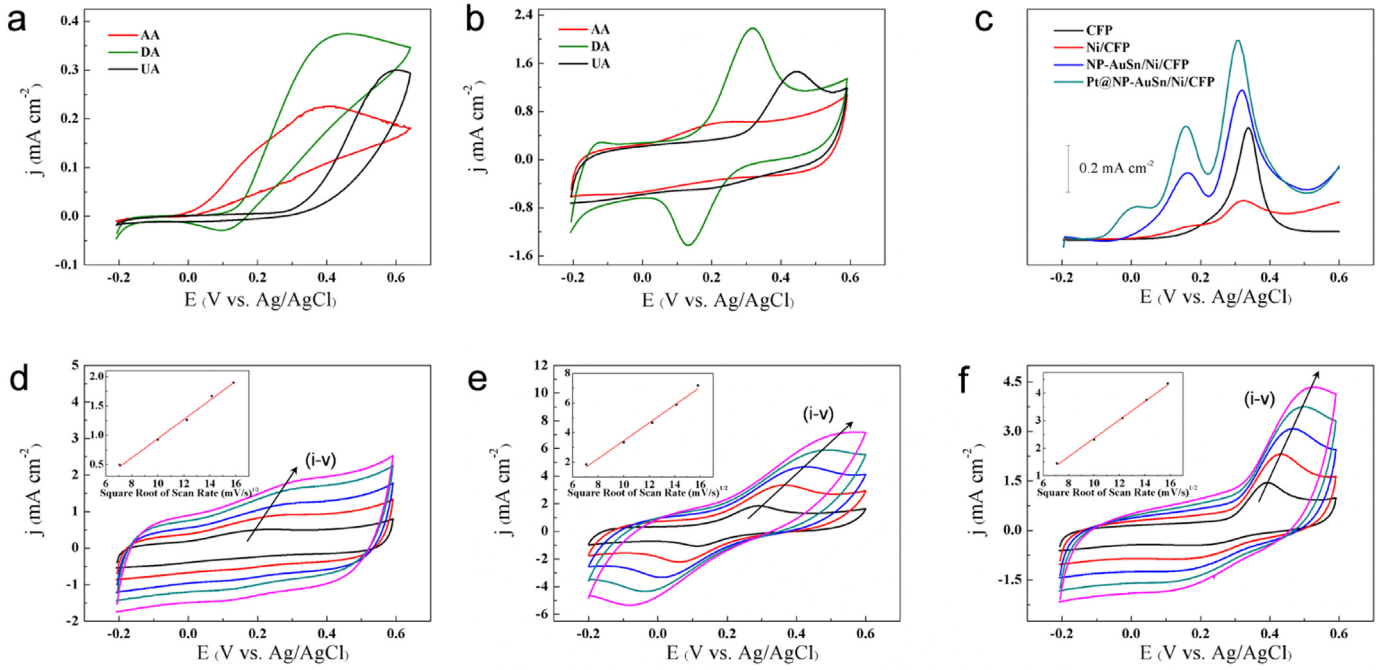

Fig. 3. CV curves of (a) CFP and (b) Pt@NP-AuSn/Ni/CFP in 0.1 M PBS (pH = 7.0) with 1 mM AA, 1 mM DA and 1 mM UA at a scan rate of 50 mV s^{-1} (c) DPV curves of CFP, Ni/CFP, NP-AuSn/Ni/CFP and Pt@NP-AuSn/Ni/CFP in the presence of 1 mM AA, 15 mM DA and 1 mM UA. (d-f) CV curves of the Pt@NP-AuSn/Ni/CFP in 0.1 M PBS (pH = 7.0) containing (d) 1 mM AA (e) 1 mM DA (f) 1 mM UA at different scan rates (50–250 mV s^{-1}). The insets show the plots of the anodic peak current *vs.* the square root of scan rate for AA, DA and UA respectively.

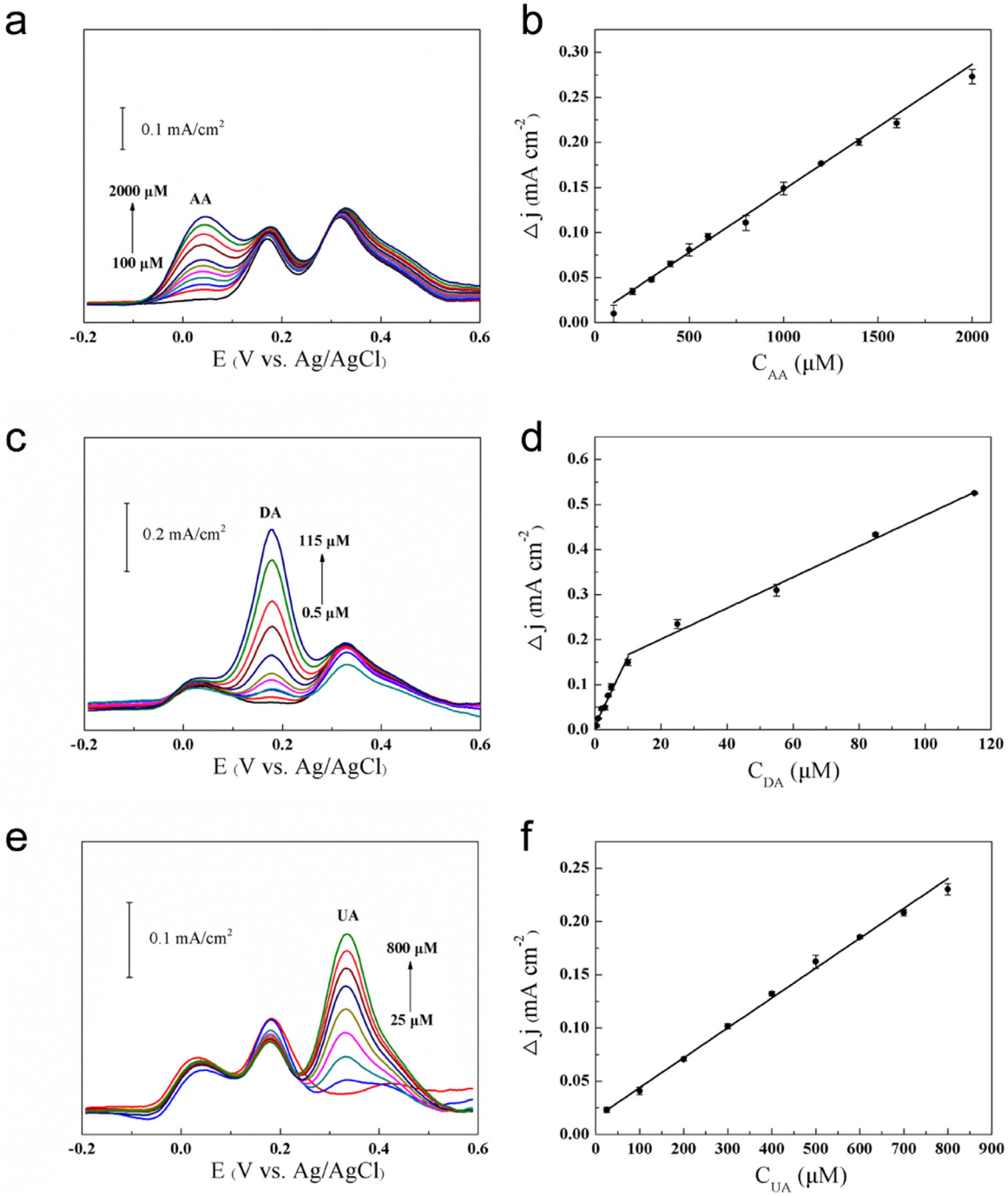

Fig. 4. DPV profiles of Pt@NP-AuSn/Ni/CFP in 0.1 M PBS (pH 7.0) containing (a) 5 μM DA, 0.5 mM UA and different concentrations of AA from 100 to 2000 μM; (c) 1 mM AA, 0.5 mM UA and different concentrations of DA from 0.5 to 115 μM; (e) 1 mM AA, 5 μM UA and different concentrations of UA from 25–800 μM. (b), (d) and (f) Corresponding plots of the anodic peak currents vs. concentrations for AA, DA and UA, in which the maximum relative standard deviations (RSDs) reach 5.1%, 4.8%, 4.3% for separated detection for AA, DA and UA.

containing 1 mM AA, 15 μM DA and 1 mM UA was also evaluated by differential pulse voltammetry (DPV). As can be seen in Fig. 3c, CFP did not show selectivity to AA, DA and UA in mixture solution. The oxidation peak of DA and UA occurred on Ni@CFP and NP-AuSn/Ni/CFP electrode, but there is no significant oxidant peak to AA. However, on Pt@NP-AuSn/Ni/CFP, oxidation peaks for AA, DA and UA were well separated and moved to more negative potential and a higher current appeared compared with NP-AuSn/Ni/CFP and Ni/CFP. These can be attributed to the fact that Pt can regulate the energy barrier of the catalytic oxidation of these three biomolecules, thereby changing the oxidation potential, so that the oxidation potential of AA, DA and UA can be separated. In addition, Pt owns superior catalytic activity for small biomolecules to NP-AuSn. Therefore, the catalytic current of the electrode can be further enhanced by the modification of Pt particles on the NP-AuSn. Fig. 3d-f shows the CV curves of the Pt@NP-AuSn/Ni/CFP at scan rates from 50 to 250 mV s^{-1} in the PBS containing 1 mM AA, 1 mM DA and 1 mM UA respectively. It can be seen that with the increase of the scan rate, the oxidation current rises. Moreover, the anodic peak current is increased with square root of scan rate (ν) linearly. The linear equations of AA, DA and UA (insets of Fig. 3d-f) can be described as: $I_{AA}=0.163*\nu^{\frac{1}{2}}-0.689$ ($R^2 = 0.9932$), $I_{DA}=0.603*\nu^{\frac{1}{2}}-2.573$ ($R^2 = 0.9919$)

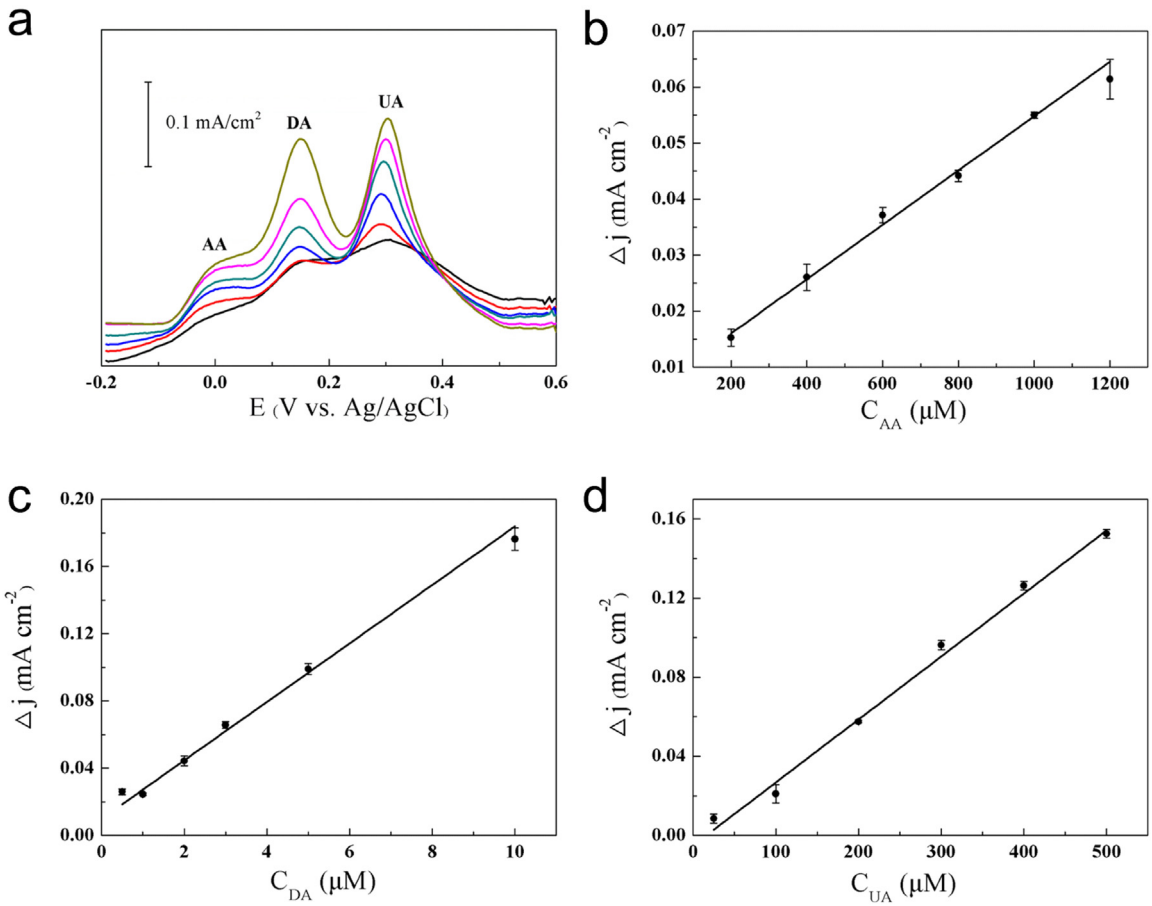

Fig. 5. (a) DPV curves on Pt@NP-AuSn/Ni/CFP in 0.1 M PBS (pH 7.0) under increasing concentrations of AA (200–1200 μM), DA (0.5–10 μM) and UA (25–500 μM) (b)-(d) Plots of the anodic peak currents vs. concentrations of AA, DA and UA respectively, where the maximum RSDs for AA, DA and UA are 5.7%, 6.7%, 8.1%, respectively.

and $I_{UA}=0.333*v^{\frac{1}{2}}-0.961$ (R^2 = 0.9976), respectively. All of these reveal that the electrochemical behaviors of AA, DA and UA on Pt@NP-AuSn/Ni/CFP were controlled by diffusion process.

In order to find the best dealloying conditions, we synthesized a series of Pt@NP-AuSn/Ni/CFP samples with different dealloying time. Fig. S7a-c shows the LSV curve of AA, DA and UA in PBS (pH = 7.0) on Pt@NP-AuSn/Ni/CFP samples dealloyed for 0–24 h. It is obvious that the oxidation current peak increase continuously with the increase of dealloying time from 0 to 20 h. When the sample was dealloyed for over 20 h, the oxidation current peak reaches the maximum and then almost keeps constant. With the progress of dealloying, the Sn content in AuSn film gradually decreases. After being dealloyed for 20 h, the Sn content keeps a relatively constant (mass fraction about 5%). Thus, the enhancement in oxidation currents for AA, DA and UA is consistent with the variation rule for Sn content in the AuSn coating obtained from the EDS measurement (Fig. S7d), which ascribes to that the decrease of the Sn content in NP-AuSn results in the increase of the porosity of NP-AuSn.

3.3. Simultaneous determination of AA, DA and UA on Pt@NP-AuSn/Ni/CFP

As discussed above, the excellent electrochemical activity of Pt@NP-AuSn/Ni/CFP electrode provides a substantial basis to simultaneous determination of AA, DA and UA. In the following measurements, the DPV method was used to determine the concentration variation for the objective biomolecule in the mixture solution containing AA, DA and UA, while the other two biomolecules were kept at a constant concentration. As shown in Fig. 4, three oxidant peaks are well-separated and located at 44 mV, 178 mV and 336 mV corresponding to the oxidation of AA, DA and UA respectively. As shown in Fig. 4a, with the successive addition of AA (200–2000 μM) in electrochemical system, the peak current near the potential at 44 mV increases while the other two peak current for DA and UA remain essentially constant. The linear equation is fitted as $I_{AA}=0.0001391*C+0.008320$ (R^2 = 0.9972), with the detection limit of 5.51 μM, as presented in Fig. 4b. Fig. 4c and Fig. 4d show the current changes and calibration plot of oxidation current versus DA concentration. With the concentration of DA increases, the oxidation current gradually increases and finally reaches the maximum. In low DA concentration region (0.5–10 μM), the fitted linear regression equation is $I_{DA}=0.01523*C+0.009940$ (R^2 = 0.9727), with the detection limits of 0.13 μM. In the high concentration region (10–100 μM), the linear regression yields a relationship of $I_{DA}=0.003340*C+0.1321$, with a correlation coefficient of R^2 = 0.9933. Similarly, as shown in Fig. 4e and Fig. 4f, the linear fitted equation of UA is $I_{UA}=0.0002805*C+0.01597$ (R^2 = 0.9979) with the detection limits of 0.67 μM. All of the detective measurements were performed under signal-to-noise ratio of S/N = 3.

The synchronous determination of AA, DA and UA was also carried out on Pt@NP-AuSn/Ni/CFP electrode by the simultaneously increasing the concentrations of the three biomolecules. As shown in Fig. 5, the oxidation peaks of AA, DA and UA were well separated in the mixed solution. In addition, as the concentration of the three molecular increases, corresponding oxidation currents gradually elevate. The linear equation of AA can be expressed as $I_{AA}=0.0004851*C+0.00632$ (R^2 = 0.9943) with the linearity range of

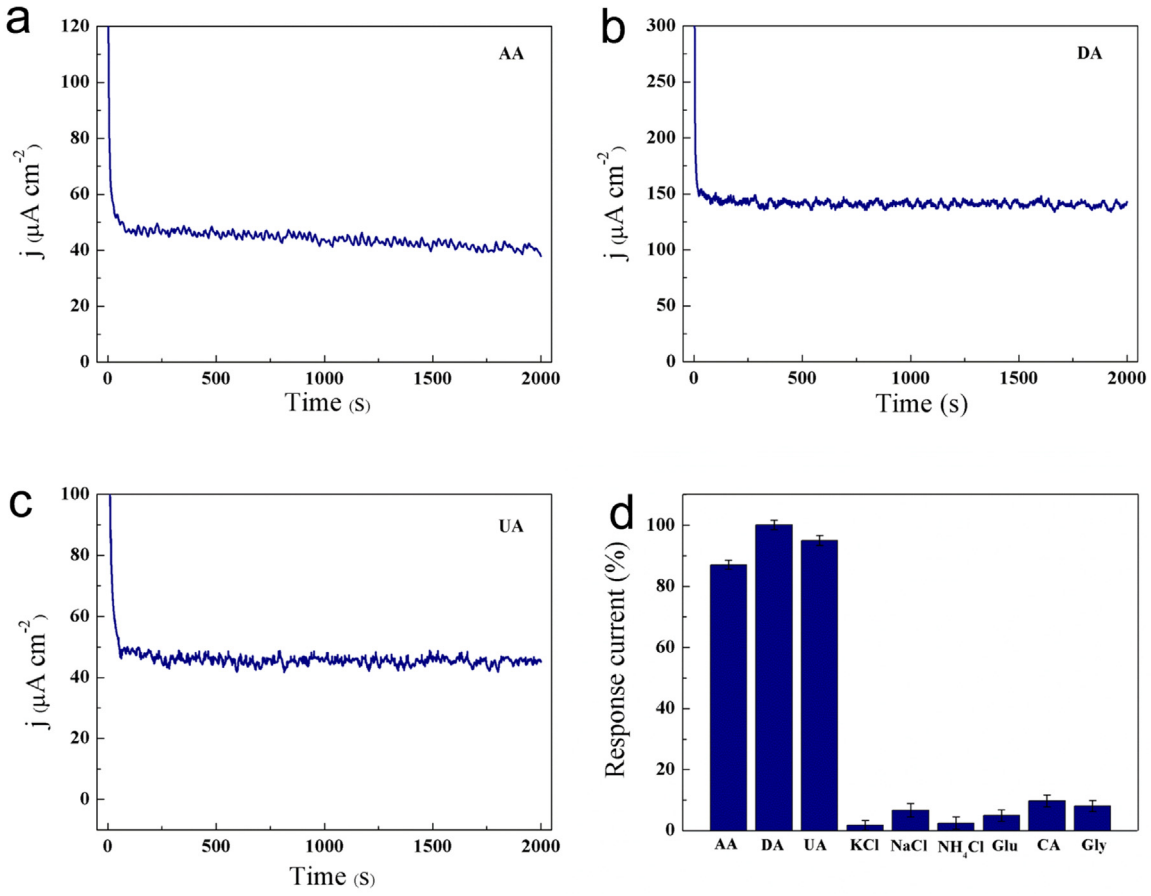

Fig. 6. The stability of the Pt@NP-AuSn/Ni/CFP in 0.1 M PBS (pH 7.0) solution containing (a) 0.5 mM AA, (b) 0.25 mM DA, and (c) 0.25 mM UA at a constant potential of 0.4 V and (d) calibrated response with addition of 10 μM UA, 10 μM AA, 10 μM DA, 100 μM KCl, 100 μM NaCl, 100 μM NH_4Cl, 1 mM glucose, 1 mM citric acid and 1 mM glycine on Pt@NP-AuSn/Ni/CFP in 0.1 M PBS (pH 7.0) at a constant potential of 0.4 V, among which the maximum RSD is 5.5%.

200–1200 μM. For DA, the linear equation is I_{DA}=0.001740*C+0.009810 (R^2 = 0.9681) (0.5–10 μM). While for UA the linear relationship between responsive current and the corresponding concentration can be described as I_{UA}=0.0003186*C−0.00511 (R^2 = 0.9926) (25–500 μM). The detection limits can reach 13.4 μM, 0.31 μM and 0.76 μM (S/N = 3) for AA, DA and UA, respectively. These results indicate that simultaneous determination AA, DA and UA was feasible on Pt@NP-AuSn/Ni/CFP electrode with high sensitivity and selectivity.

3.4. The stability and anti-interference for the detection of UA, DA and AA

Stability is an important indicator for evaluation of the long-term operation ability of the sensor to detect AA, DA and UA. Thus, chronoamperometry was used to measure the continuous operation of Pt@NP-AuSn/Ni/CFP at 0.40 V for 0.50 mM AA, 0.25 mM DA and 0.25 mM UA in 0.1 M PBS (pH = 7.0), respectively. It's obvious that Pt@NP-AuSn/Ni/CFP possesses excellent stability for UA, DA and AA detection. As shown in Fig. 6a-c, the AA, DA and UA signals were reduced by 6.6%, 2.7% and 3.1% after operation for 2000 s. In addition, anti-interference ability was also studied under common interferents to simulate the actual complex environment in practical detection. Glucose, citric acid, KCl, NaCl, glycine and NH_4Cl were chosen to work as interferents for AA, DA and UA detection since they considerably exist in body fluids. As shown in Fig. S8, 10 μM UA, 10 μM AA, 10 μM DA, 10-fold concentration ratio of KCl, NaCl, NH_4Cl and 100-fold concentration ratio of glucose, citric acid (CA), glycine were successively added into 0.1 M PBS (pH 7.0) buffer at the potential of 0.40 V. There is no significant change for oxidation current with these interferents. Comparison of current response for DA detection with AA, UA and interfering species is illustrated by histogram in Fig. 6d. The result presents that these interferents presented below 10% current change compared to DA, AA and UA. All of results above demonstrate that the as-prepared Pt@NP-AuSn/Ni/CFP electrode possesses a high selectivity and a reliable anti-interference property.

3.5. Real samples analysis

In order to evaluate the practical application of the Pt@NP-AuSn/Ni/CFP, the electrode was used for the detection of AA, DA and UA in urine sample using standard addition method. The urine sample was diluted 50-fold with 0.1 M PBS (pH 7.0) without other pretreatment process. It is shown in Table S3 that AA, DA and UA in ternary mixtures could be detected with the appropriate recovery. The relative standard deviation (RSD) is less than 5% and the recovery is between 95% and 105%. These results confirm that the electrode has the reliability and great potential for the simultaneous detection of AA, DA and UA in actual samples.

4. Conclusions

In summary, a novel hierarchical Pt@NP-AuSn/Ni/CFP was successfully fabricated by replacement reaction between H_2PtCl_6 and nanoporous AuSn film on Ni buffered carbon fiber paper. Coating a layer of Ni between electrodeposited Au-Sn alloy and CFP can effectively solve the problems of film uniformity and weak adhesion between An-Sn alloy layer and substrate. Due to the advantages of large surface area of nanoporous metal, macroporous carbon fiber paper facilitating mass

transfer and excellent electrocatalytic activity of Pt@NP-AuSn, high sensitivity and wide detection limit for simultaneous measurement of AA, DA and UA were obtained. Moreover, Pt@NP-AuSn/Ni/CFP also shows long-term sensing stability towards the AA, DA and UA detection. Excellent selectivity was observed with little influence under the presence of KCl, NaCl, NH_4Cl with 10-fold concentration and glucose, citric acid, glycine with 100-fold concentration. All in all, The Pt@NP-AuSn/Ni/CFP electrode manifests great potential as a candidate of electrochemical sensors for AA, DA and UA simultaneous sensing.

Acknowledgement

Dr. G. Cui and J. Zhao gratefully acknowledges the financial support by National Natural Science Foundation of China (51271205, 50801070, 51571093), Excellent young college teacher development program in Guangdong province (Yq2013006), "Research and Application of Key Technologies Oriented the Industrial Development" (90035-3283309, 90035-3283321), "Project of Science and Technology Plan" by Guangzhou city (2013Y2-00102), and by Chinese Central Authority University Fund (2015ZM094, 16lgjc6). This work was also supported by National Nature Science Foundation of China, China (21622509, 21475122, 21527806), Department of Science and Techniques of Jilin Province (20160201008GX), Jilin Province Development and Reform Commission (2016C014 and 2017C053-1), Science and Technology Bureau of Changchun (15SS05).

Appendix A. Supporting information

Supplementary data associated with this article can be found in the online version at doi:10.1016/j.bios.2018.10.012.

References

Abellán-Llobregat, A., Jeerapan, I., Bandodkar, A., Vidal, L., Canals, A., Wang, J., Morallón, E., 2017a. Biosens. Bioelectron. 91, 885–891.
Abellán-Llobregat, A., Vidal, L., Rodríguez-Amaro, R., Berenguer-Murcia, Á., Canals, A., Morallón, E., 2017b. Electrochim. Acta 227, 275–284.
Cai, W., Lai, J., Lai, T., Xie, H., Ye, J., 2016. Sens. Actuators B: Chem. 224, 225–232.
Cherevko, S., Kulyk, N., Chung, C.H., 2012. Langmuir 28, 3306–3315.
Deng, W., Yuan, X., Tan, Y., Ma, M., Xie, Q., 2016. Biosens. Bioelectron. 85, 618–624.
Feng, J., Zhao, W., Su, B., Wu, J., 2011. Biosens. Bioelectron. 30, 21–27.
Gao, G., Zhang, Z., Wang, K., Yuan, Q., Wang, X., 2017. Nanoscale 9, 10998–11003.
Hua, Z., Liu, Y., Yao, G., Wang, L., Ma, J., Liang, L., 2012. J. Mater. Eng. Perform. 21, 324–330.
Huang, C.T., Chen, M.L., Huang, L.L., Mao, I.F., 2002. Chin. J. Physiol. 45, 109–115.
Huang, Y., Miao, Y.E., Ji, S., Tjiu, W.W., Liu, T., 2014. ACS Appl. Mater. Interfaces 6, 12449–12456.
Jiang, J., Du, X., 2014. Nanoscale 6, 11303–11309.
Jindal, K., Tomar, M., Gupta, V., 2014. Biosens. Bioelectron. 55, 57–65.
Kalimuthu, P., John, S.A., 2010. Talanta 80, 1686–1691.
Ke, X., Xu, Y., Yu, C., Zhao, J., Cui, G., Higgins, D., Chen, Z., Li, Q., Xu, H., Wu, G., 2014a. J. Mater. Chem. A 2, 16474–16479.
Ke, X., Xu, Y., Yu, C., Zhao, J., Cui, G., Higgins, D., Li, Q., Wu, G., 2014b. J. Power Sources 269, 461–465.
Khan, M.M.I., Haque, A.M.J., Kim, K., 2013. J. Electroanal. Chem. 700, 54–59.
Kim, S.J., Cho, Y.K., Lee, C., Kim, M.H., Lee, Y., 2016. Biosens. Bioelectron. 77, 1144–1152.
Kim, S.J., Kim, Y.L., Yu, A., Lee, J., Lee, S.C., Lee, C., Kim, M.H., Lee, Y., 2014. Sens. Actuators B: Chem. 196, 480–488.
Lang, X., Hirata, A., Fujita, T., Chen, M., 2011. Nat. Nanotechnol. 6, 232–236.
Levine, M., Dhariwal, K.R., Washko, P.W., Butler, J.D., Welch, R.W., Wang, Y., Bergsten, P., 1991. Am. J. Clin. Nutr. 54, 1157S–1162S.
Li, Y., Song, H., Zhang, L., Zuo, P., Ye, B. ce, Yao, J., Chen, W., 2016. Biosens. Bioelectron. 78, 308–314.
Lin, K.C., Tsai, T.H., Chen, S.M., 2010. Biosens. Bioelectron. 26, 608–614.
Liu, Z., Wu, Z.S., Yang, S., Dong, R., Feng, X., Müllen, K., 2016. Adv. Mater. 28, 2217–2222.
Mirčeski, V., Lovrić, M., 2004. J. Electroanal. Chem. 565, 191–202.
Sun, C.L., Chang, C.T., Lee, H.H., Zhou, J., Wang, J., Sham, T.K., Pong, W.F., 2011a. ACS Nano 5, 7788–7795.
Sun, C.L., Lee, H.H., Yang, J.M., Wu, C.C., 2011b. Biosens. Bioelectron. 26, 3450–3455.
Teymourian, H., Salimi, A., Khezrian, S., 2013. Biosens. Bioelectron. 49, 1–8.
Wang, Z., Yang, M., Chen, C., Zhang, L., Zeng, H., 2016. Sci. Rep. 6, 29611.
Xia, Y., Huang, W., Zheng, J., Niu, Z., Li, Z., 2011. Biosens. Bioelectron. 26, 3555–3561.
Xiao, X., Conghaile, P., Leech, D., Ludwig, R., Magner, E., 2017. Biosens. Bioelectron. 90, 96–102.
Xu, Y., Ke, X., Yu, C., Liu, S., Zhao, J., Cui, G., Higgins, D., Chen, Z., Li, Q., Wu, G., 2014. Nanotechnology 25, 445602.
Yang, Y.J., Li, W., 2014. Biosens. Bioelectron. 56, 300–306.
Yue, H.Y., Huang, S., Chang, J., Heo, C., Yao, F., Adhikari, S., Gunes, F., Liu, L.C., Lee, T.H., Oh, E.S., Li, B., Zhang, J., Huy, T.Q., Luan, N., Van, Lee, Y.H., 2014. ACS Nano 8, 1639–1646.
Zhang, C., Lai, C., Zeng, G., Huang, D., Tang, L., Yang, C., Zhou, Y., Qin, L., Cheng, M., 2016a. Biosens. Bioelectron. 81, 61–67.
Zhang, C., Xiao, J., Qian, L., Yuan, S., Wang, S., Lei, P., 2016b. J. Mater. Chem. A 4, 9502–9510.
Zhao, D., Fan, D., Wang, J., Xu, C., 2015. Microchim. Acta 182, 1345–1352.
Zhao, D., Yu, G., Tian, K., Xu, C., 2016. Biosens. Bioelectron. 82, 119–126.